Available online at www.sciencedirect.com
SCIENCE DIRECT®
Journal of Chromatography B, 808 (2004) 43–50
JOURNAL OF CHROMATOGRAPHY B
www.elsevier.com/locate/chromb

Affinity parameters of amino acid derivative binding to molecularly imprinted nanospheres consisting of poly[(ethylene glycol dimethacrylate)-co-(methacrylic acid)]

Mathias Lehmann, Melanie Dettling, Herwig Brunner, Günter E.M. Tovar*

Fraunhofer Institute for Interfacial Engineering & Biotechnology and Institute for Interfacial Engineering, University of Stuttgart, Nobelstr. 12, 70569 Stuttgart, Germany

Available online 6 May 2004

Abstract

The binding of L-Boc-phenylalanine anilide (BFA) and L-Boc-phenylalanine (phe) to molecularly imprinted and non-imprinted polymer nanoparticles consisting of poly[(ethylene glycol dimethacrylate)-co-(methacrylic acid)] has been investigated by adsorption experiments and mathematical modeling. The experimental isotherms have been mathematically adapted following the models of Freundlich, Langmuir, Langmuir–Freundlich, Bi-Langmuir, and extended Langmuir. The extended Langmuir model differentiated between specific and nonspecific binding of the ligand to the receptor nanoparticles and rendered excellent fitting of the experimental data. It delivered a thermodynamic and kinetic parameter set on the experimental association curves of L-BFA by L-BFA-imprinted nanospheres in suspension experiments with the equilibrium constant $K_D = 4.09 \pm 0.69\,\mu mol\,L^{-1}$ and the kinetic association rate constant $k_a = 5.60\,mL\,\mu mol^{-1}\,min^{-1}$.

Keywords: Molecular recognition; Adsorption isotherm; Amino acids; Molecularly imprinted nanospheres; Poly[(ethylene glycol dimethacrylate)-co-(methacrylic acid)]

1. Introduction

There has been an increasing interest in the synthesis and characterization of molecularly imprinted polymers (MIP's) as synthetic affinity material lately [1–4]. Molecular imprinting is a template polymerization which induces receptor-like binding sites in otherwise non-selective polymeric materials. Thus, adsorbent material is created which can hold highly specific binding sites towards the template molecule used during the imprinting process. A large variety of different chemical compounds have been successfully used as molecular templates in non-covalent imprinting processes, including amino acids, drugs, fertilizers, biocides and peptides [1–4]. The use of MIP's as solid selector phase have been demonstrated for many applications, e.g. in liquid chromatography [5], capillary electro chromatography [6,7], solid-phase extraction [8–10], or membrane processes [11,12].

Recently, the synthesis of MIP's in a colloidal format was realized by hetero-phase polymerization processes [13]. We employed miniemulsion polymerization and prepared nanoscopic MIP's (nanoMIP's) in a one-stage reaction [14,15], whereas Perez et al. and Carter and Rimmer used a two-stage emulsion polymerization to prepare colloidal core-shell MIP's with an imprinted shell [16–18]. Colloidal MIP's exhibiting a perfectly spherical morphology. Due to the nanoscopic size of the imprinted particles they posses a high specific surface of $80\,m^2g^{-1}$ [19]. Thus, colloidal MIP's are more defined in their topology as conventional MIP polymer material which is synthesized by bulk synthesis with applying a porogen and is then ground to render particles of irregular shape and a size of several tens of micrometers.

In contrast, our nanoMIP's represent a solid phase selector which can be handled in a liquid without limitation by sedimentation processes. Furthermore, nanoMIP's can be deposited as (ultra)thin layers in composite membranes [19,20] or sensor coatings [21]. For optimal design of such affinity membranes or sensors, the knowledge of the thermodynamic and kinetic properties of the molecular recognition

* Corresponding author. Tel.: +49-711-970-4109; fax: +49-711-970-4200.
E-mail address: guenter.tovar@igb.fraunhofer.de (G.E.M. Tovar).

1570-0232/$ – see front matter © 2004 Elsevier B.V. All rights reserved.
doi:10.1016/j.jchromb.2004.03.068

process of a target molecule by the molecularly imprinted material is indispensable.

Affinity adsorption processes employing specific adsorbent–adsorbate (receptor–ligand) systems, were experimentally investigated and mathematically modeled by various approaches, e.g. for optimization of analytical affinity chromatography [22,23] or particle-based and membrane affinity processes [24]. The bulk imprinting processes applied, yielded a distribution of binding sites having a range of binding affinities [25,26]. This heterogeneity diminishes the abilities of MIP's in almost every analytical application. Thus, the reduction of heterogeneity in MIP's would significantly improve their overall utility. Essential requirement toward this end are new synthetic routes to MIP's but also the ability to accurately characterize the binding properties of MIP's [25,27].

Heterogeneity also complicates the characterization of MIP's; therefore, the majority of binding models have been homogeneous models that enable the facile estimation of binding parameters. A bi-Langmuir isotherm has been most commonly employed to describe the slope analysis of Scatchard plots [28–31]. Here, the heterogeneity of the MIP binding sites is approximated by grouping the heterogeneous distribution into two classes; one of low and one of high affinity. Alternative models are focusing on the combination of Freundlich and Langmuir models [27] or the complete numerical calculation of affinity distribution of MIPs [26,32,33].

Therefore, in the present contribution, we report on adsorption experiments and their mathematical modeling by various binding models to compare and study the thermodynamic and kinetic behavior of the binding process of nanoMIP's consisting of poly[(ethylene glycol dimethacrylate)-co-(methacrylic acid)] (*p*(EGDMA-co-MAA)) with the template molecule used in the imprinting process, L-BOC-phenylalinine anilide (L-BFA). Non-imprinted *p*(EGDMA-co-MAA) nanospheres were used as control material and L-Boc-phenylalanine (L-phe) as template analogue for comparative adsorption studies. In addition to the understanding of the employed nanoMIP's binding properties, main goal of the mathematical modeling is the determination of reasonable parameter sets for the further use in engineering the optimum separation process with nanoMIP's as selective stationary phase in thin film composite membranes [19,20].

2. Experimental and modeling

2.1. NanoMIP synthesis

The nanospheres were synthesized by miniemulsion polymerization. For a detailed description see elsewhere [34]. Briefly, this polymerization corresponded to a oil-in-water polymerization using strong shear forces to transform oil droplets to nanodroplets of the size range of 50–300 nm diameter. These nanodroplets, stabilized by sodium dodecylsulfate (SDS, Merck, Darmstadt, Germany), served as nanoreactors, containing ethylene glycol dimethacrylate (EGDMA, Sigma, Taufkirchen, Germany), methyacrylic acid (MAA, Aldrich, Taufkirchen, Germany), the template L-Boc-phenylalanine anilide (BFA, Novabiochem, Schwalbach, Germany), and hexadecane (Fluka, Taufkirchen, Germany). The latter was a hydrophobic additive stabilizing the nanodroplets during the miniemulsion polymerization. The nanodroplets were quantitatively converted to solid nanospheres with an efficiency of 98 ± 2%. After the polymerization the nanospheres were purified by ultrafiltration (Amicon 8400 ultrafiltration cell, polysulfone membrane, PALL GmbH, Dreieich, Germany) and the template was removed by extraction.

2.2. Adsorption experiments

For determination of the adsorption isotherms the following experiment were carried out. Equal amounts of nanospheres (20 mg) were added to eight flasks containing various concentrations (10, 20, 30, 40, 50, 60, 70 and 80 μM) of adsorbent molecule in water–methanol solution (75:25, v/v) in a final volume of 50 mL. The solvent composition was chosen because of the advantageous equilibration distribution, i.e. sufficient solubility of BFA and high affinity to the imprints of the nanoMIP's. The concentration range is obviously low compared to data reported for other templates dissolved in purely organic solvents with concentrations up to 3 M [35,36]. In our case, the solubility of the L-BFA molecules in the water–methanol solution limited the range.

The flasks were stirred at room temperature with a magnetic stirrer at 450 rpm for at least 4 h in order for the system come to equilibrium. Samples (2 mL) were removed and cleaned from the nanospheres with a syringe filter (PTFE membrane, 0.2 μm, Achroma, Müllheim, Germany).

To demonstrate that the syringe filter itself does not adsorb the compounds, blank experiments were carried out. Therefore a sample of each flask containing various concentrations (10, 20, 30, 40, 50, 60, 70 and 80 μM) of adsorbent molecule was processed through the syringe filter without any particles prior to the adsorption experiment and the template concentration was determined. The amount of template molecules in the supernatant after all filtering experiments was determined by measuring the absorbance at 240 nm (BFA) and 220 nm (phe) with an HPLC system equipped with an UV-Vis-spectrometer (Beckman Coulter, Munich, Germany).

In order to determine the association rate constant k_a, the following batch procedure was used: The amount of 20 mg of extracted molecularly imprinted nanospheres was suspended in water–methanol solution (75:25, v/v) in a final volume of 50 mL and an initial adsorbent concentration of 45 μM. The flasks were stirred at room temperature with a magnetic stirrer at 450 rpm. Thirteen samples were taken continuously

at defined time intervals (after 1, 2, 3, 4, 6, 8, 10, 15, 20, 40, 60, 90 and 120 min). The last sample was taken after 2 h when the equilibrium was achieved, as evidenced by the lack of further reduction in the concentration of adsorbent in the soluble phase.

2.3. Theory of adsorption isotherm modeling

When a solute or adsorbate (A) in a reaction mixture adsorbs to a solid phase or adsorbent which contains specific binding sites (B), the binding is described by Eq. (1), where k_a and k_d are the rate constants for the forward and backward direction of the reaction.

$$A + B \underset{k_d}{\overset{k_a}{\rightleftharpoons}} AB \tag{1}$$

In the present case the specific binding sites correspond to molecularly imprinted sites at the nanoMIP's. The ratio of the constants is equal to the dissociation equilibrium constant K_D, given in Eq. (2).

$$K_D = \frac{k_d}{k_a} \tag{2}$$

An additional term, given in Eq. (3), for the mass of nonspecifically bound molecules c_N was assumed to be in linear correlation to the free adsorbate after equilibration in the soluble phase [37,38]. By other means, as long as free surface is available during the adsorption process, the nonspecific binding will unabatedly take place parallel to the specific adsorption until the equilibrium is reached:

$$c_N = Nc^* \tag{3}$$

By combining Eq. (3) with the traditional Langmuir isotherm model for single-solute adsorption [39] the values of the equilibrium constant K_D, the maximum number of binding sites c_m and the rate of nonspecific binding N were determined with the following Eq. (4).

$$c_S = \frac{c^* c_m}{K_D + c^*} + Nc^* \tag{4}$$

The complete amount of template molecule bound to the imprinted nanospheres c_S was calculated as the total amount of template molecule present at the beginning of the adsorption isotherm experiment c_0 less the amount still in the soluble phase at equilibrium c^*. The fitting was done iteratively by using the software Aspen Custom Modeler (Aspentech, Cambridge, USA) which allows generating a fast solution without complex data preparation.

2.4. Theory of kinetical modeling

The rate of mass transfer to the high specific binding sites of the adsorbent in the affinity interaction is given by Eq. (5).

$$\frac{dc_H}{dt} = \underbrace{k_a c(c_l - c_H)}_{\text{adsorption}} - \underbrace{k_d c_H}_{\text{desorption}} \tag{5}$$

The rate constant for desorption of the adsorbate molecule k_d from the imprints of the nanospheres was replaced by Eq. (2) governing the following expression.

$$\frac{dc_H}{dt} = k_a c(c_l - c_H) - K_D k_a c_H \tag{6}$$

Except the adsorption rate constant k_a all other variables are known from the batch isotherm experiment done before. The rate of mass transfer of the nonspecific binding to the free surface of the adsorbent characterized by Eq. (3) is given by Eq. (7)

$$\frac{\partial c_L}{\partial t} = k_L c - \frac{k_L}{N} c_L \tag{7}$$

whereas k_L is the rate constant for nonspecific binding in forward direction. To correctly involve the nonspecific adsorption to the imprinted nanospheres, a mass balance has to be established. The entire mass of adsorbate is constituted from the dissolved molecules and the adsorbate molecule bound specifically and nonspecifically to the imprinted nanospheres, where V is the volume of the soluble phase, V_{MIP} the volume of the solid-phase and ρ_{MIP} the density of the solid phase, i.e. the molecularly imprinted nanospheres. With the boundary condition in terms of the time $t > 0$ the following Eq. (8) is used:

$$V(c_0 - c) = V_{MIP}\rho_{MIP}(c_H + c_L) \tag{8}$$

Eqs. (6–8) were solved in the modeling process using the software Aspen Custom Modeler (Aspentech, Cambridge, USA) to match the experimental data of the kinetic batch adsorption experiments without further modification.

3. Results and discussion

Binding experiments were carried out by suspending a constant amount of nanoMIP's or non-imprinted controls in a solution consisting of water and methanol (75:25, v/v), which contained a constant concentration of L-Boc-phenylalanine anilide (BFA) or L-Boc-phenylalanine (phe). To obtain experimental data on the equilibrium state, the initial adsorbate concentration in the suspending solution was varied. After incubation, the nanoparticles of the sample were removed by filtration and the ligand concentration in the water–methanol phase was determined by HPLC three times for each sample. To demonstrate that the filter itself does not adsorb the compounds, blank experiments were carried out. The template concentration in the samples prior to and after the filtering process remained constant within 99.1%. Thus, it was concluded that any adsorption of the template by the syringe filter could be neglected.

Here four different types of adsorbent–adsorbate systems were employed: BFA-imprinted nanoMIP's with BFA (system 1) or phe (system 2), and non-imprinted *p*(EGDMA-co-MAA) nanoparticles with BFA (system 3) or phe (system 4).

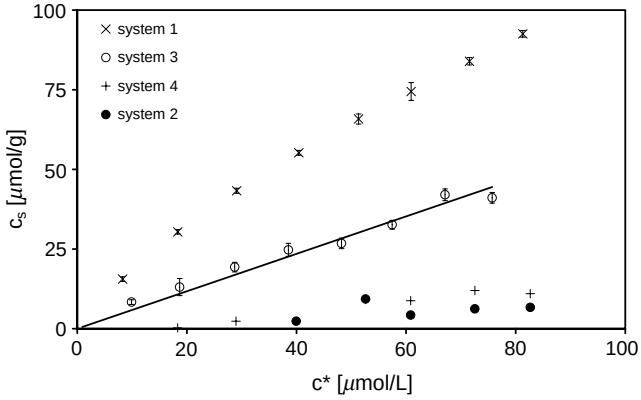

Fig. 1. Experimental data of the adsorption isotherm experiments employing BFA-imprinted nanoMIP's with L-BFA (system 1) or Boc-L-phenylalanine (phe) (system 2), and non-imprinted *p*(EGDMA-co-MAA) nanoparticles with BFA (system 3) or phe (system 4). Error bars span two-fold the observed standard deviation, and points without error bars were measured only once.

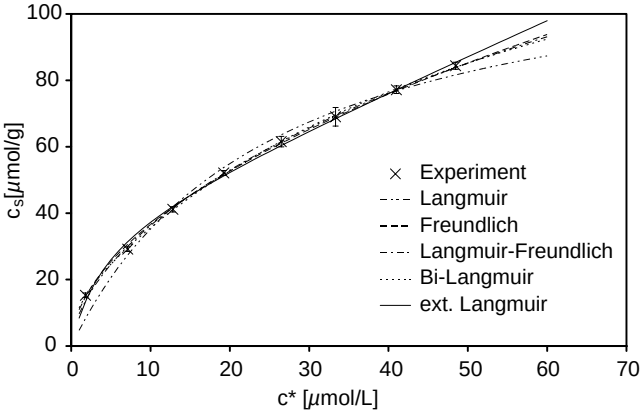

Fig. 2. Five binding models (Freundlich, Langmuir, Langmuir–Freundlich, Bi-Langmuir and extended Langmuir) together with the experimental data of affinity system 1.

The experimental data on the adsorption isotherm experiments with the affinity system and the various control systems are illustrated in Fig. 1. The affinity system 1 showed the highest amount of L-BFA adsorption to the L-BFA-imprinted nanospheres. Thus, it was confirmed, that an increased affinity was generated between the imprinted polymer and the adsorbate which was used as molecular template for its imprinting. However, the control system 3 showed also a substantial adsorption of BFA under the same conditions. This adsorption was by definition attributed to nonspecific binding as no specific ligand-receptor interaction due to an imprinting process could have been involved in this case. The data on both other controls, the adsorbent–adsorbate systems 2 and 4, displayed very low nonspecific adsorption to the nanospheres. Taken all data into account, it was stated, that the adsorbate molecule BFA exhibited a stronger interaction with the copolymer nanoparticles consisting of *p*(EGDMA-co-MAA) as the compared adsorbate phe. Most importantly, the imprinting process induced the generation of specific binding sites in the material thus leading to an increased adsorption of the adsorbate BFA to BFA-imprinted nanoparticles. Five different models have been applied for the mathematical modeling of the experimental data.

Fig. 2 and Table 1 show the resulting fitting parameters by employing the equation systems based on the isotherm models Freundlich (FM), Langmuir (LM), Bi-Langmuir (BLM), Langmuir–Freundlich (LFM) and extended Langmuir (ELM). The traditional Freundlich model (FM) allows for the description of a broad range of affinity interactions by assuming a hypothetic association constant and an heterogeneity index but no information about a maximum number of available binding sites. Here, the model produced a theoretical curve, which was in good agreement with the experimental data on the BFA adsorption to BFA-imprinted nanoparticles [40]. The calculated heterogeneity index of 0.52 already pointed out that there was not only one kind of attractive interaction in the investigated ligand-receptor system. In contrast, the classical Langmuir isotherm (LM) postulates only one possible type of interaction between the ligand and the receptor, i.e. just specific binding sites [41]. When the LM was applied to fit the experimental data, a clear deviation of the theoretical curve from the experimental data was found. Thus it was concluded, that the simple LM was not appropriate to describe the adsorption behavior in the investigated case, which was already found by Shimizu and co-workers for other MIP systems [27]. A combination of both models, the Freundlich–Langmuir model (FLM), was successfully applied to MIP systems at different concentration ranges and

Table 1
Fitted affinity parameters using different models from literature and the extended Langmuir model together with the appropriate correlation coefficient *R*

Model	Parameter		Correlation *R*
Freundlich	$\bar{K}_D = 0.01 \pm 0.0008\,\mu M$; $m = 0.52 \pm 0.01$		0.9985
Bi-Langmuir (Scatchard)	High: $K_D = 0.60 \pm 0.36\,\mu M$ Low: $K_D = 14.37 \pm 2.38\,\mu M$	$c_m = 62.16 \pm 9.11\,\mu mol\,g^{-1}$ $c_m = 159.21 \pm 9.20\,\mu mol\,g^{-1}$	0.9998
Langmuir–Freundlich	$K_D = 741.13 \pm 772.64\,\mu M$; $m = 0.59 \pm 0.04$	$c_m = 510.97 \pm 307.58\,\mu mol\,g^{-1}$	0.9994
Langmuir	$K_D = 25.14 \pm 4.38\,\mu M$; $c_m = 123.98 \pm 9.94\,\mu mol/g$		0.9917
Extended Langmuir	$K_D = 4.09 \pm 0.69\,\mu M$; $c_m = 37.75 \pm 2.64\,\mu mol/g$	$N = 1.06 \pm 0.05\,L\,g^{-1}$	0.9981

affinity distributions [27]. Fig. 2 shows a good agreement of the fit curve based on the FLM but the values of the parameters c_m and K_D and their resulting standard deviations displayed in Table 1, where by far too high to render reliable parameters for describing the investigated affinity system. The Bi-Langmuir model (BLM) differentiates between two types of binding sites, one with high affinity and one with low affinity [30,42]. The application of the BLM rendered a well fitting theoretical curve. However, the mathematical model in this case is based on the assumption of an overall maximum number of affinity binding sites of 221.37 μmol g^{-1}, which is by far too high if compared to the overall maximum number binding sites available by experimental extraction of the imprinted nanoparticles with methanol of 120.09 μmol g^{-1}. Furthermore, when the observed linear increase of nonspecific binding of BFA to non-imprinted *p*(EGDMA-co-MAA) nanospheres is taken into account (Fig. 1), we concluded, that the nonspecific binding would be better modelled by introduction of a linear term depending only on the ligand concentration in the investigated concentration regime [37,38]. Thus, instead of assuming precisely two different types of specific binding sites, as in the BLM, the extended Langmuir model (ELM) differentiated between a specific interaction based on the molecular recognition of the adsorbate with specific binding sites in the adsorbent generated by molecular imprinting and all other interactions between adsorbate and adsorbent subsumed as nonspecific binding, were modelled by two mathematically independent terms. The ELM described the experimentally observed adsorption processes excellently. Furthermore, the value of 37.75 ± 2.64 μmol g^{-1} for the maximum number of binding sites, which was determined by the modeling based on the ELM, is more reasonably related to the amount of extracted template. This value corresponds to 31.4% of the amount of extracted template, which is assumed to be the proportion of easily accessible imprinted binding sites. Furthermore, the ELM rendered by far more reasonable parameters for describing the binding behaviour of BFA to *p*(EGDMA-co-MAA) nanospheres as the FM, which provided a hypothetic value for a mean equilibrium constant with no relation to any number of binding sites. Thus, it was concluded, that the ELM described the binding events upon BFA binding to imprinted *p*(EGDMA-co-MAA) nanospheres most precisely.

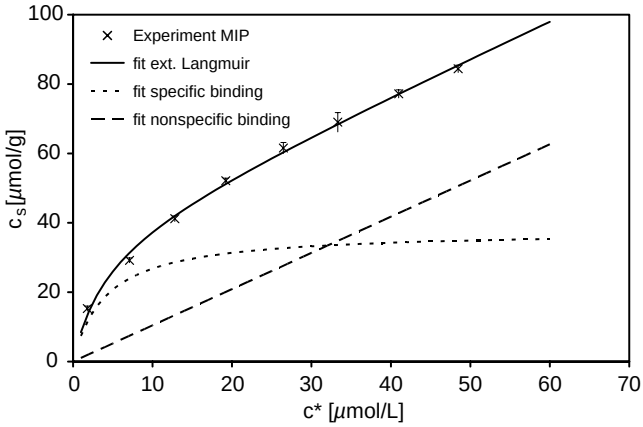

Fig. 3. Best fitting functions matching the experimental data of the affinity system 1, BFA adsorbing to BFA-imprinted nanoMIP's: adsorption fit using the full modified Langmuir model (—); a linearly increasing function attributed to the nonspecific adsorption (- - -); the adsorption function describing the specific adsorption due to molecular recognition of the adsorbate in the imprinted binding sites (· · ·).

Fig. 3 displays the mathematical functions resulting from the iterative fitting procedure according to the extended Langmuir model together with the experimental adsorption data. The ELM modeling resulted in a function describing the overall adsorption process which coincided fully with the experimental data. The function consisted of a linearly increasing term describing the nonspecific binding and a Langmuir adsorption isotherm term describing the specific binding converging against the maximum specific adsorbate binding capacity c_m. Table 2 shows the full parameter set rendered by the best fitting of the experimental data observed with the system 1 and its control system 3 based on the ELM.

The determined an equilibrium constant for the BFA binding to BFA-imprinted nanospheres, K_D = (4.09 ± 0.69) μmol L^{-1}, agreed well with the data range reported for other molecularly imprinted affinity systems [40]. Sergeyeva et al. found a K_D = (80.0 ± 10) μmol L^{-1} for the affinity of terbumeton to a photo-grafted terbumeton-imprinted membrane coating consisting of poly(MAA-co-*N*,*N*′-methylene-bis-acrylamide) [43]. Yoshikawa et al. reported a K_D = 103.0 μmol L^{-1} for the affinity of acetyl-L-tryptophan to Boc-L-tryptophan-imprinted polymer membranes consisting of a blend of peptide modified resins with *p*(acrylonitrile-co-styrene) [44].

Table 2
Fitted parameters equilibrium constant K_D, the maximum number of specific binding sites c_m, and the rate of nonspecific binding *N* by using the extended Langmuir model differentiating between two independent terms, one describing the molecular recognition of the adsorbate by the nanoMIP's based on specific binding to imprinted sites and the other subsuming nonspecific interactions

Affinity system	K_D (μmol L^{-1})	c_m (μmol g^{-1})	*N*/L (g^{-1})
BFA with BFA-imprinted nanosphere (system 1)	4.09 ± 0.69	37.75 ± 2.64	1.06 ± 0.05
BFA with nanospheres (system 3)			
non-imprinted	6.43 ± 18.75	8.03 ± 10.23	0.60 ± 0.14
BFA with non-imprinted nanospheres (system 3); only nonspecific binding assumed	–	0	0.55 ± 0.03

The linear dependence of the nonspecific binding used in the modeling was confirmed by fitting the experimental data observed with the control system 3, where BFA was adsorbed to non-imprinted nanospheres. Free iterative fitting of the ELM Eq. (4) resulted in fictive values for K_D and c_m (Table 2). The standard deviation of the fictive equilibrium constant describing a fictive specific binding in the system was about three times higher than the calculated equilibrium constant itself, thus confirming the validity of the ELM. Consequently, in a more realistic modeling of the control system, the theoretical maximum specific adsorbate binding capacity c_m was set to 0, and thus any fictive specific adsorption excluded from the modeling. Thereby, the rate describing the nonspecific binding changed only slightly and was calculated to 0.55 ± 0.03, (Table 2). When this value was compared to the rate in the imprinted system, we found a ratio of $N_{\text{imprinted}}/N_{\text{non-imprinted}} = 1.93$. The rate of nonspecific binding N depends on the available surface in the nanosphere system. Thus, the found ratio of 1.93 should be mirrored by different specific surfaces of the imprinted and non-imprinted nanospheres. It was shown earlier, that the specific surface of the imprinted and non-imprinted particles was almost unaffected by their chemical composition, but was largely increased upon extraction of the template [14]. The nanoparticles investigated here, showed almost the same size with an average diameter of 240 and 255 nm for system 1 (imprinted particles) and system 3 (non-imprinted particles), respectively. Their corresponding specific surfaces as measured by nitrogen BET adsorption measurements were 49 and 52 m^2g^{-1} for system 1 and 3, respectively. Upon extraction with a good solvent, here methanol, only the specific surface of the imprinted system 1 changed significantly to 64 m^2g^{-1}. The ratio of their resulting specific surfaces, specific surface of system 1 divided by the specific surface of system 3, yields a value of 1.23. Although the specific surface determined by the BET adsorption experiments using nitrogen molecules differed principally from the surface available for adsorption of the larger BFA, it may still be regarded as a good measure to attribute the calculated differences in nonspecific binding rates for the imprinted and non-imprinted nanospheres.

The excellent agreement of the ELM allowed for applying the determined thermodynamic parameter set on the mathematical modeling of kinetic data to describe the adsorption process. Fig. 4 shows experimental data on kinetic measurements of single-solute adsorption processes for the systems 1 and 2 together with calculated association curves in terms of the free BFA concentration. The calculated association curves described the experimental data with excellent agreement. The modeled curve for the adsorption in the system 1 correlated with a coefficient of $R = 0.9987$. The adsorption kinetics of the affinity system 1 showed a strong decrease in the first minutes. After about 20 min the adsorption was nearly completed, reflected by a very slow decay in the modeled association curve. Equilibrium was reached after 30 min. In contrast to these findings, the free concentration of the adsorbate in the control system 2 showed no significant change and thus indicated the lack of affinity to the BFA-imprinted nanospheres. Additionally, Fig. 5 shows experimental data on kinetic measurements of single-solute adsorption processes for the systems 1 and 2 together with calculated association curves in terms of the overall, specific and nonspecific binding of BFA based on Equations (6), (7) and (8). Comparing the curves for the modeled specific and nonspecific bindings shows, that after 20 min almost all specific binding sites are saturated at 32 $\mu mol\,g^{-1}$ whereas the slower nonspecific binding needs up to 80 min to reach a constant plateau of 25 $\mu mol\,g^{-1}$. Thus, an association rate constant k_a for the specific binding was determined for the affinity system 1 to $k_a = 5.6\,mL\,\mu mol^{-1}\,min^{-1}$ and for the nonspecific binding to $k_L = 45.5\,mL\,g^{-1}\,min^{-1}$ by the mathematical fitting using the previously determined adsorption isotherm parameters listed in Table 1.

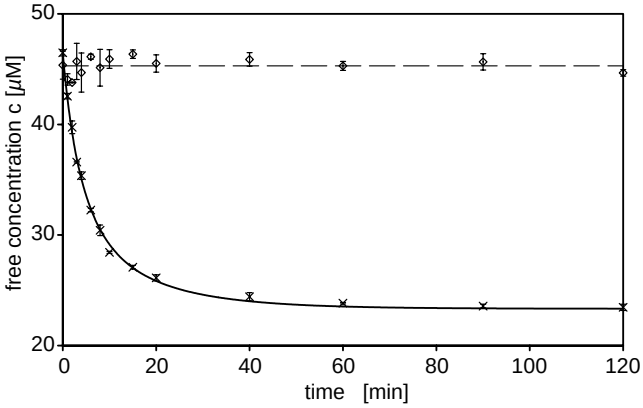

Fig. 4. Modeling of single-solute association curves describing the experimental data of the free concentration on kinetic measurements of adsorption processes: Systems 1, BFA adsorption to BFA-imprinted nanoMIP's (×××); system 2, phe adsorption to BFA-imprinted nanoMIP's (◇◇◇), together with the appropriate modelled values of the system 1 (—) and system 2 (- - -). Error bars span 2 standard deviations.

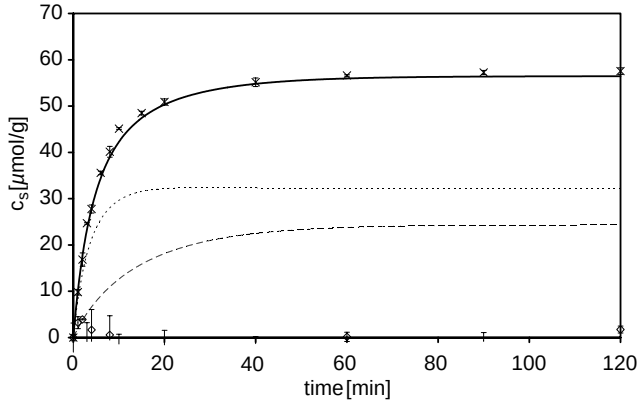

Fig. 5. Modeling of single-solute association curves describing the experimental data of the bound BFA on kinetic measurements of adsorption processes: Systems 1, BFA adsorption to BFA-imprinted nanoMIP's (–×–); system 2, phe adsorption to BFA-imprinted nanoMIP's (◇◇◇), together with the modelled values of the specific (· · ·) and nonspecific (- - -) binding. Error bars span 2 standard deviations.

4. Conclusions

An extended Langmuir model (ELM) was used to fit the experimental data of BFA adsorption to L-BFA-imprinted nanospheres consisting of *p*(EGDMA-co-MAA) taking into account independent terms describing the specific and nonspecific binding in this affinity system within the chosen concentration range. The parameters rendered by the model covered the values of the dissociation equilibrium constant K_D, the association rate constants k_a and k_L, the maximum number of binding sites c_m, and the parameter N, expressing the rate of nonspecific binding. The comparison of the ELM with other models showed an almost exact agreement concerning the affinity parameters indicating the good performance of the chosen model. The thermodynamic and kinetic data are important to describe the affinity process involved in the adsorbate-adsorbent interaction in the case of molecularly imprinted nanospheres. Moreover, we previously reported about the making of an affinity composite membrane containing a thin layer of the nanoMIP's as selective phase [19,20]. The governed thermodynamic and kinetic parameters can now be used together with the continuity equation [37], to establish a new mathematical model for the understanding and describing of the whole separation process by such a composite membrane. Thus, with the mathematical modeling, it should be possible to predict e.g. the breakthrough curves and the influence of axial diffusion of such a separation process leading to an optimal configuration and therefore optimal performance of the envisaged composite membrane in the expected narrow concentration range.

5. Nomenclature

A	adsorbate
B	adsorbent binding site
BFA	BOC-L-phenylalanine anilide
BLM	vi-Langmuir model
c	solute concentration [μmol L^{-1}]
c^*	solute concentration at equilibrium [μmol L^{-1}]
c_0	initial solute concentration [μmol L^{-1}]
c_m	maximum number of available binding sites per solid mass [μmol g^{-1}]
c_L	amount of nonspecifically bound adsorbate per solid mass [μmol g^{-1}]
c_H	amount of specifically bound adsorbate per solid mass [μmol g^{-1}]
c_S	complete amount of bound adsorbate per solid mass [μmol g^{-1}]
ELM	extended Langmuir model
FM	Freundlich model
FLM	Freundlich–Langmuir model
K_D	dissociation equilibrium constant [μmol L^{-1}]
k_a	association rate constant [mL μmol^{-1} min^{-1}]
k_d	dissociation rate constant [min^{-1}]
k_L	nonspecific association rate constant [mL g^{-1} min^{-1}]
LM	Langmuir model
m	heterogeneity index [−]
MIP	molecularly imprinted polymer
N	rate of nonspecific binding [L g^{-1}]
phe	phenylalanine
ρ_{MIP}	density of molecularly imprinted nanospheres [g L^{-1}]
R	correlation coefficient
t	time [min]
V	volume of soluble phase [L]
V_{MIP}	solid phase volume of molecularly imprinted nanospheres [L]

Acknowledgements

The authors thank Christiane Renner for experimental help with the adsorption experiments. G.E.M.T. thanks the German Federal Ministry for Education and Research (BMBF), the "Fraunhofer-Gesellschaft", and the "Land Baden-Württemberg" for financial support of a junior research group ("Nachwuchsforschergruppe") on "Biomimetic Interfaces".

References

[1] M.J. Whitcombe, E.N. Vulfson, Adv. Mater. 13 (2001) 467.
[2] B. Sellergren, Angewandte Chemie 112 (2000) 1071.
[3] L.I. Andersson, J. Chromatogr. B 739 (2000) 163.
[4] H. Asanuma, T. Hishiya, M. Komiyama, A. Mater. 12 (2000) 1019.
[5] M. Kempe, K. Mosbach, J. Chromatogr. A 691 (1995) 317.
[6] L. Schweitz, L.I. Andersson, S. Nilsson, Anal. Chim. Acta 435 (2001) 43.
[7] P.T. Vallano, V.T. Remcho, J. Chromatogr. A 887 (2000) 125.
[8] L.I. Andersson, A. Paprica, T. Arvidsson, Chromatographia 46 (1997) 57.
[9] C. Berggren, S. Bayoudh, D. Sherrington, K. Ensing, J. Chromatogr. A 889 (2000) 105.
[10] Y.B. Chen, M. Kele, P. Sajonz, B. Sellergren, G. Guiochon, Anal. Chem. 71 (1999) 928.
[11] J. Mathew-Krotz, K.J. Shea, J. Am. Chem. Soc. 118 (1996) 8154.
[12] S.A. Piletsky, T.L. Panasyuk, E.V. Piletskaya, I.A. Nicholls, M. Ulbricht, J. Membr. Sci. 157 (1999) 263.
[13] B. Sellergren, A.J. Hall, in: B. Sellergren (Ed.), Molecularly Imprinted Polymers, Elsevier, Amsterdam, 2001, p. 21.
[14] D. Vaihinger, K. Landfester, I. Kräuter, H. Brunner, G.E.M. Tovar, Macromol. Chem. Phys. 203 (2002) 1965.
[15] A. Weber, M. Dettling, H. Brunner, G.E.M. Tovar, Macromol. Rapid Commun. 23 (2002) 824.
[16] N. Pérez, M.J. Whitcombe, E.N. Vulfson, J. Appl. Polymer Sci. 77 (2000) 1851.
[17] N. Pérez, M.J. Whitcombe, E.N. Vulfson, Macromolecules 34 (2001) 830.
[18] S.R. Carter, S. Rimmer, Adv. Mater. 14 (2002) 667.
[19] M. Lehmann, H. Brunner, G.E.M. Tovar, Desalination 149 (2002) 315.
[20] M. Lehmann, H. Brunner, G.E.M. Tovar, Chemie Ingenieur Technik 75 (2003) 149.

[21] G.E.M. Tovar, C. Gruber, M. Dettling, S. Sezgin, M. Lehmann, A. Weber, H. Brunner, in: F.W. Scheller (Ed.), Proceedings of the Third Biosensor Symposium, University of Potsdam, Potsdam, Germany, 2003, p. 31.
[22] F.H. Arnold, S.A. Schofield, H.W. Blanch, J. Chromatogr. 355 (1986) 1.
[23] F.H. Arnold, H.W. Blanch, C.R. Wilke, Chem. Eng. J. 30 (1985) B9.
[24] M. Unarska, P.A. Davies, M.P. Esnouf, B.J. Bellhouse, J. Chromatogr. 519 (1990) 53.
[25] R.J. Umpleby, M. Bode, K.D. Shimizu, Analyst 125 (2000) 1261.
[26] A.K. Thakur, P.J. Munson, D.L. Hunston, D. Rodbard, Anal. Biochem. 103 (1980) 240.
[27] R.J. Umpleby, S.C. Baxter, Y. Chen, R.N. Shah, K.D. Shimizu, Anal. Chem. 73 (2001) 4584.
[28] G. Vlatakis, L.I. Andersson, R. Müller, K. Mosbach, Nature 361 (1993) 645.
[29] J.-D.V. Loon, R.G. Janssen, W. Verboom, N. David, Tetrahedron Lett. 33 (1992) 5125.
[30] K.J. Shea, D.A. Spivak, B. Sellergren, J. Am. Chem. Soc. 115 (1993) 3368.
[31] P. Sajonz, M. Kele, G. Zhong, B. Sellergren, G. Guiochon, J. Chromatogr. A 810 (1998) 1.
[32] D.L. Hunston, Anal. Biochem. 63 (1975) 99.
[33] C.H. Reinsch, Numerische Mathematik 10 (1967) 177.
[34] D. Vaihinger, K. Landfester, I. Kräuter, H. Brunner, G.E.M. Tovar, Macromol. Chem. Phys. 203 (2002) 1965.
[35] Z. Jie, H. Xiwen, Anal. Chim. Acta 381 (1999) 85.
[36] S.H. Cheong, A.E. Rachkov, J.K. Park, K. Yano, I. Karube, J. Appl. Polymer Sci. A 36 (1998) 1725.
[37] S.-Y. Suen, J. Chem. Technol. Biotechnol. 70 (1997) 278.
[38] G. Cutsforth, V. Koppaka, S. Krishnaswamy, J. Wu, K. Mann, B. Lentz, Biophys. J. 70 (1996) 2938.
[39] E.L. Cussler, Diffusion, Cambridge University Press, Cambridge, 1997.
[40] R.J. Umpleby, S.C. Baxter, M. Bode, J.K. Berch Jr., R.N. Shah, K.D. Shimizu, Anal. Chim. Acta 435 (2001) 35.
[41] I. Langmuir, J. Am. Chem. Soc. 40 (1918) 1361.
[42] L.I. Andersson, R. Mueller, G. Vlatakis, K. Mosbach, Proc. Natl. Acad. Sci. USA 92 (1995) 4788.
[43] T.A. Sergeyeva, H. Matuschewski, S.A. Piletsky, J. Bendig, U. Schedler, M. Ulbricht, J. Chromatogr. A 907 (2001) 89.
[44] M. Yoshikawa, T. Ooi, J. Izumi, Euro. Polymer J. 37 (2001) 335.